Colloids and Surfaces A: Physicochemical and Engineering Aspects 624 (2021) 126776

Contents lists available at ScienceDirect

Colloids and Surfaces A: Physicochemical and Engineering Aspects

journal homepage: www.elsevier.com/locate/colsurfa

In situ encapsulation of rivastigmine in TAT-functionalized P(MMA-co-AA) nanoparticles through miniemulsion polymerization

L.H.R. Mangia [a], H.C. Ferraz [a,*], R.S.D. Souza [b], M.C.S. Pereira [b], J.C. Pinto [a]

[a] Programa de Engenharia Química/COPPE, Universidade Federal do Rio de Janeiro (UFRJ), Cidade Universitária, CP:68502, Rio de Janeiro, 21941-972 RJ, Brazil
[b] Laboratório de Ultraestrutura Celular, Instituto Oswaldo Cruz (Fiocruz), Rio de Janeiro, Brazil

GRAPHICAL ABSTRACT

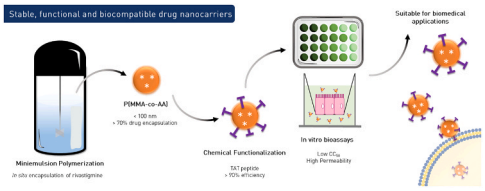

ARTICLE INFO

Keywords:
Encapsulation
Rivastigmine
Poly(methyl methacrylate-co-acrylic acid)
Chemical functionalization
Miniemulsion polymerization
Alzheimer disease

ABSTRACT

The present study aimed to encapsulate rivastigmine (a drug used for treatment of the Alzheimer disease) in poly (methyl methacrylate – co – acrylic acid), P(MMA-co-AA), nanoparticles functionalized with the transcription activator peptide (TAT) for biomedical applications. Encapsulation was performed *in situ* through miniemulsion polymerization at different preparation conditions and the highest encapsulation efficiencies (around 80%) were obtained when the comonomer mixture contained 7.5 wt% of acrylic acid in methyl methacrylate. Afterwards, functionalization trials of the previously prepared polymer nanoparticles were performed through chemical adsorption, leading to high TAT immobilization efficiencies (94%). Additionally, toxicity bioassays conducted with Caco-2 cells monolayers revealed that the cytotoxicity of obtained particles was low and did not depend on the nanoparticle composition. Besides, the obtained results indicated that the functionalized nanoparticles could cross the intestinal epithelial barrier successfully. Finally, the obtained particles presented good stability, could be prepared with high encapsulation and functionalization efficiencies, and presented advantageous biological properties that encourage the future development of biomedical uses.

1. Introduction

The Alzheimer Disease (AD) is a complex neurodegenerative disorder that is responsible for nearly 60–70% of the cases of dementia, and constitutes an enormous challenge for individuals, families and health professionals, being the fifth leading cause of death among the elderlies [1–4]. The highest risk factor associated with the AD progress is aging [3,5]. Given the present social scenario, characterized by the reduction of global fertility and rise of life expectancy, the number of AD patients is expected to rise in the following decades [1,3,4]. In fact, it is estimated that the cases of AD (and other types of dementia) will nearly triple by 2050, affecting 115 million people worldwide [4,6]. The socioeconomic impact of the disease is also a major concern, given the impressive number of US$ 290 billion related to AD treatments in 2019, only in the

* Correspondence to: Programa de Engenharia Química/COPPE, Universidade Federal do Rio de Janeiro (UFRJ).
E-mail address: helen@peq.coppe.ufrj.br (H.C. Ferraz).

https://doi.org/10.1016/j.colsurfa.2021.126776
Received 5 February 2021; Received in revised form 25 April 2021; Accepted 28 April 2021
Available online 5 May 2021

USA, estimated by the Alzheimer's Association [7]. Therefore, the development of effective therapeutic strategies for AD treatment is needed urgently.

The original causes of AD are still unknown and despite all the efforts that have been made to develop therapeutic strategies to prevent (and halt) the progression of the disease, the obtained results have not been satisfactory so far [1,8–10]. The modulation of neurotransmitters by drugs constitutes the most favorable alternative for health improvement of AD patients [1]. To date, few drugs have been approved by the Food and Drug Administration (FDA) to treat AD symptoms: donepezil, galantamine and rivastigmine as acetylcholinesterase inhibitors (AchEI), and memantine [1,4,9,10]. It is important to observe that the use of rivastigmine can affect positively two acetylcholine regulatory enzyme systems; thus it can be regarded as an efficient pharmacological treatment for AD at the present moment [11,12]. However, the use of AchEI has been constantly associated with various adverse effects, such as nausea, vomiting, diarrhea, dizziness and weight loss [12,13]. Therefore, the development of more efficient drugs with lower adverse effects constitutes a promising area of study in the field of AD treatment. One strategy under development is the manufacture and use of nanocarriers for optimization of drug delivery, reduction of adverse effects and increase of bioavailability [14–17].

The use of nanocarriers has been widely investigated in controlled drug delivery applications, allowing better therapeutic results through regulation of temporal and spatial distribution of the drug in the body. Additionally, nanocarriers can protect the drug from degradation or complete elimination by the body, favoring transport by physiological barriers and driving the drug to the place of action, minimizing adverse effects in other regions of the body [18,19]. Among the various possible types of nanocarriers, polymer nanoparticles can be regarded as promising and efficient multivalent drug vehicles for various biomedical applications. The main advantages of polymer nanoparticles can be associated with the high versatility of the molecular and morphological characteristics of these materials, which can provide interesting and specific properties for the delivery application and encapsulation of the drug. In addition, the easy insertion of functional groups at the nanoparticle surfaces can allow the proper design of the targeting properties, facilitating particle diffusion through natural physiological barriers and increasing the drug concentration at the desired site of action [14,20,21].

In the case of AD treatment, the Blood Brain Barrier (BBB) constitutes a physiological barrier for the Central Nervous System (CNS), presenting long extension and high selectivity. It is generally accepted that the BBB is the most important barrier for transportation of molecules into the brain, constituting a major challenge for development of therapeutic strategies that depend on delivery of drugs into the brain [21,22]. Particularly, Kreuter et al. (2014) pointed out that nanoparticles can be transported through the BBB by receptor-mediated transcytosis. Therefore, it may be possible to deliver nanoparticles into the brain if they are functionalized with specific binders that can interact with the BBB surface receptors [16,21]. For this reason, many studies investigated the use of different types of ligands (surfactants, insulin, transferrin, endothelial antibodies, among others) to promote the internalization of nanoparticles into the brain tissue [16,21–25].

It is believed that the functionalization of nanoparticles with cell-penetrating peptides (CPP) can stimulate the transport through the BBB and simultaneously reduce the cellular toxicity [22,26]. As a matter of fact, several CPPs can enhance the permeability of external agents through the BBB, including transcription activator peptides (TAT), Angiopep, penetratin, SynB, glycoprotein of rabies virus, among others. Particularly, Rao et al. (2008) showed that the use of TAT-conjugated nanoparticles could increase the drug concentration levels in the brain 800 times, when compared to drug administration in solution. Additionally, the authors showed that nanoparticles could also be used to keep the rate of drug release constant in the brain for long periods of time [27].

Based on the previous paragraphs, the present study aimed to encapsulate rivastigmine in poly(methyl methacrylate – co – acrylic acid), P(MMA-co-AA), nanoparticles functionalized with TAT for development of a possible treatment for AD in the future. The polymer matrix was selected in the present work because it is nontoxic, biocompatible and already used in many biomedical applications safely [28,29], constituting a good model for experimentation. Besides, the polymer matrix can be biodegradable when copolymerized with other comonomers [30–32]. It is important to emphasize that acrylic acid provides carboxylic acid groups that can be used for functionalization and supporting of TAT molecules.

In the present study, *in situ* encapsulation was performed through miniemulsion polymerization at different preparation conditions. Miniemulsion polymerizations have been frequently used for drug encapsulation because the operation can be performed in a single step with very high encapsulation efficiencies [33–35]. Afterwards, functionalization of the previously prepared polymer nanoparticles was performed through chemical adsorption [36]. Moreover, toxicity bioassays were conducted with Caco-2 cells monolayers to characterize the cytotoxicity of obtained nanoparticles, which were also used for analyses of permeability through an intestinal epithelial barrier.

2. Materials and methods

2.1. Materials

2.1.1. Polymerization reactions

Rivastigmine free basis was purchased from Carbosynth (Berkshire, United Kingdom) with minimum purity of 98 wt%. Methyl methacrylate (MMA) and acrylic acid (AA) were acquired from Sigma Aldrich (Rio de Janeiro, Brazil) with minimum purities of 99.5 wt% and 99 wt%, respectively. The surfactant sodium dodecyl sulfate (SDS) and the initiator potassium persulfate (KPS) were purchased from Vetec Química Fina (Rio de Janeiro, Brazil) with minimum purity of 90 wt% (containing 10 wt% of water). Sodium bicarbonate was acquired from Proquimios (Rio de Janeiro, Brazil) with minimum purity of 99 wt%. The co-stabilizer n-hexadecane and hydroquinone used purchased from Vetec Química (Rio de Janeiro, Brazil) with minimum purities of 99.5 wt % and 99 wt%, respectively. Tetrahydrofuran (THF) was used as mobile phase for gel permeation chromatography (GPC) analyses and was purchase from Tedia (Rio de Janeiro, Brazil) with minimum purity of 99 wt%).

2.1.2. Functionalization

Lysine (lys, minimum purity of 98 wt%), TAT HIV-1 peptide (TAT, minimum purity of 98 wt%), bovine serum albumin (BSA, minimum purity of 98 wt%), 2-aminobenzamide (ABZ, minimum purity of 98 wt %), 1-ethyl-3-(3-dimethylaminopropyl)-carbodiimide (EDC, minimum purity of 97 wt%), Bradford reagent (minimum purity of 98 wt%) and o-phthaldialdehyde (OPA, minimum purity of 98 wt%) were purchased from Sigma Aldrich (Rio de Janeiro, Brazil).

2.1.3. Biological assays

Caco-2 cells line derived from human colon adenocarcinoma (ATCC HTB-37TM), GIBCO Dulbecco's modified eagle's medium, glucose, fetal bovine serum (FBS), glutamine, commercial solution of penicillin and streptomycin, trypsin (standard reference), Triton X-100, paraformaldehyde and ethylenediaminetetraacetic acid (EDTA) solution were purchased from Sigma Aldrich (Rio de Janeiro, Brazil) with minimum purity of 98.5 wt%. The phosphate saline buffer (PBS) pH 7.4 was prepared with sodium chloride, dibasic sodium phosphate and hydrated monobasic sodium phosphate supplied by Sigma Aldrich (Rio de Janeiro, Brazil) with minimum purity of 99 wt%. Anti-tight junction protein 1 (zona occludens 1) antibody (anti-ZO1) and 1,4-diazabicyclo [2.2.2]octane (DABCO) were purchased from Sigma Aldrich (Rio de Janeiro, Brazil) with minimum purity of 99 wt%. CellTiter-Blue® cell

viability assay kit was acquired from Promega Corporation (Madison, USA). Sterile 96-well white bottom acrylic plates, Corning® Transwell® cell culture polyester membranes and 75 cm^2 TPP® sterile culture flasks were provided by Sigma Aldrich (Rio de Janeiro, Brazil).

2.2. Polymerization reactions

PMMA and P(MMA-co-AA) nanoparticles were prepared by mini-emulsion polymerization as described by Campos, Ferraz and Pinto (2016). The aqueous/oil mass ratio was equal to 80/20. The aqueous phase contained SDS (1 wt%), KPS (0.1 wt%), sodium bicarbonate (0.08 wt%) and distilled water. The organic phase contained n-hexadecane (0.08 wt%) and monomers (AA and MMA), with AA concentrations of 7–15 wt%. When present, rivastigmine free base was added to the organic phase at concentrations of 0.5 wt%, 1.0 wt% and 1.5 wt%. The initial miniemulsion was prepared with a sonicator (Vibra Cell VCX 750 model, Sonics & Materials Inc. Newtown, USA) working with amplitude of 40% at 20 kHz for 5 min. Then, the miniemulsion was transferred to a glass reactor vessel (Easy Max 102 model, Mettler Toledo, Ohio, USA) of 100 mL where the polymerization reaction was carried out at 80 °C, under continuous agitation of 500 rpm for 2 h.

Monomer conversions were evaluated through gravimetric analyses. At specified sampling times, aliquots of 1 mL were collected and mixed with 1 mL of a previously prepared hydroquinone solution (1 wt%) to halt the reaction. Then, collected samples were dried in a recirculating oven at 40 °C until constant weight.

Particle size distributions were characterized through dynamic light scattering using a ZetaSizer Nano ZS equipment (Malvern Instruments, Malvern, United Kingdom) using latex samples diluted in distilled water (1:500 in volume). Average particle diameters and polydispersity indexes (PDI) were automatically calculated and reported as averages of 100 readings of three distinct measurements. The zeta potential was characterized through electrophoretic light scattering using the same equipment.

Polymers samples were characterized through Fourier-transform infrared spectroscopy (FT-IR), gel permeation chromatography (GPC) and nuclear magnetic resonance (NMR). FT-IR analyses were conducted with dried samples in the spectral range between 400 and 4000 cm^{-1} with resolution of 4 cm^{-1} using a Nicolet 6700 FT-IR spectrometer (Thermo Fisher Scientific, Massachusetts, USA) equipped with an ATR Smart Orbit accessory. The final spectra were reported as averages of 128 scans, automatically calculated by the equipment.

GPC analyses were performed with a Viscotek Max VE2001 chromatograph (Malvern Instruments, Malvern, United Kingdom), equipped with a refractometer detector (model Viscotek VE 3580, Malvern Instruments, Malvern, United Kingdom), and a set of linear Shodex columns (KF-G pre column, followed by one KF-805L column and two KF-804L columns, all of them from Showa Denko K.K., Tokyo, Japan). A calibration curve was performed with polystyrene standards with molecular weights ranging from 376 to 1×10^6 Da. The polymer samples were prepared at 1 mg/mL in THF and the injection volume was equal to 200 µL. All analyses were performed using constant flow rate of 1.0 mL/min at 40 °C.

H NMR analyses were conducted in solutions of deuterated chloroform on the AVIII-500 equipment (Bruker, Massachusetts, USA), using a 5-mm probe at frequency of 500 MHz.

Drug encapsulation efficiencies (EE%) were evaluated through characterization of drug concentrations in the supernatant after centrifugation of 3 mL of latex samples using a Megafuge 16R centrifuge (Thermo Fisher Scientific, Massachusetts, USA) and an Amicon Ultra-15 Membrane 100KDa (Millipore, Massachusetts, USA) device at 6000 rpm for 20 min. Rivastigmine concentrations were evaluated through UV–VIS spectrophotometric analyses (UV-M51 spectrometer, BEL Engineering, Milano, Italy) and using a standard curve built at the wavelength of 263 nm.

2.3. Nanoparticle functionalization

Functionalization was performed through chemical reaction between the free carboxylic acid groups of P(MMA-co-AA) nanoparticles and the amino groups of the biomolecule. In the present study, two different conjugates were used: lysine and TAT. The immobilization reaction was performed as recommended by Hermanson (2008) and Campos, Ferraz and Pinto (2016).

Firstly, 1 mL of the latex was added to 1.5 mL of EDC solution (0.05 mol/L) in 0.1 M of the phosphate buffer (pH 6.7) and kept under agitation for 2 h at 20 rpm in Roto-Shake Genie mixing device (Scientific Industries Inc., New York, USA). Afterwards, the suspension was centrifuged for 10 min at 6000 rpm with an Amicon Ultra-15 Membrane 100KDa (Millipore, Massachusetts, USA), and the filtrated nanoparticles were suspended in 1 mL phosphate buffer. Then, bioconjugation was performed through the addition of 40 mg of lysine or 0.45 mL of TAT solution (2.5 g/L) in phosphate buffer, followed by an incubation period of 2 h under 20 rpm in the same mixing device. Finally, the centrifugation procedure was repeated and the functionalization efficiency was evaluated through characterization of unabsorbed protein in the supernatant phase by UV–VIS spectrophotometric analyses. Unreacted lysine concentration was titrated in accordance with the OPA protocol at 340 nm [37], while unreacted TAT concentration was characterized through standard Bradford analyses at 595 nm [38] using a BSA standard curve. The solid phase was dried in recirculation oven at 30 °C and characterized through FT-IR analyses in order to confirm the immobilization through chemical adsorption.

For *in vitro* tests, the nanoparticles were also functionalized as described before, except that in the bioconjugation step 0.20 mL of TAT solution (2.5 g/L) and 0.5 mL ABZ (20 mg/mL) buffer solutions were added in order to incorporate both protein binding and fluorescent feature to the nanoparticles.

2.4. Cytotoxicity and permeability analyses

Caco-2 cells monolayers (ATCC HTB-37™), cultivated in culture flasks with area of 75 cm^2, were dissociated with a trypsin/EDTA solution. The isolated cells were seeded at density of 1.5×10^4 cells/well in 96-well white clear bottom plates. Then, cells were grown for 4 days at 37 °C and 5% CO_2 in high-glucose Dulbecco's modified eagle medium (DMEM) supplemented with fetal bovine serum (10 wt%). The confluent cells were treated with encapsulated rivastigmine (0.11–250 µg encapsulated rivastigmine/mL) for 72 h at 37 °C. Untreated cells and cells dosed with empty nanoparticles (without rivastigmine) were used as control references. Cell viability was determined through quantitation of ATP using Celltitter Glo kit (Promega Corporation, Wisconsin, USA). The luminescence signal was measured with a FlexStation-3 equipment (Molecular Devices, Sunnyvale, USA). The concentration that reduced 50% of the cell viability (CC_{50}) was determined by linear regression.

Cellular permeability assays were performed with Caco-2 cells (2×10^5 cells/well) grown for 4 days in Transwell® (Sigma Aldrich, Rio de Janeiro, Brazil). Confluent monolayers were incubated on upper chamber with 100 µg nanoparticles/mL of P(MMA-co-AA) functionalized with ABZ. After 4 h, the medium from the lower chamber was removed and the permeability calculated by fluorescence readings in SpectraMax 190 Microplate Reader (Molecular Devices, California, USA). Non-encapsulated nanoparticles, EDTA treated and untreated cells were used as control references. Additionally, the Transwell membranes were removed from the insert and processed for tight junction detection.

2.5. Indirect immunofluorescence

Caco-2 cells monolayers incubated or not with the nanoparticles were fixed for 20 min at 4 °C with 4% paraformaldehyde in PBS pH 7.4. After fixation, the cells were washed and permeabilized with 0.5%

Triton X-100. After blocking, the cells were incubated overnight at 4 °C with anti-ZO1 antibody (1:200). Then, the cells were washed and incubated for 1 h at 37 °C with the appropriate secondary antibody. Samples were mounted with DABCO and observed with help of a Zeiss Axio Imager M2 fluorescence microscope (Zeiss, Oberkochen, Germany).

3. Results and discussion

3.1. Particle characterization

Table 1 shows the average particle diameters, zeta potential and drug encapsulation efficiencies of the products obtained after the polymerization reactions, confirming that nanosized particles were prepared through miniemulsion polymerizations. Additionally, the obtained nanoparticles presented similar average diameters, smaller than 100 nm and in the range between 65 and 80 nm (Table 1), which are consistent and in accordance with previous studies regarding the preparation of P (MMA-co-AA) nanoparticles [39]. Moreover, the small and similar diameter values of the obtained particle, along with the simplicity of the proposed *in situ* encapsulation technique highlight the importance of the reported findings, as hydrophobic rivastigmine has not been considered very often in encapsulation studies [15,17,40–44]. According to Elsabhy and Wooly (2013), nanoparticles with average sizes ranging from 10 to 100 nm can be handled safely and are appropriate for the desired therapeutic applications [20]. Therefore, the obtained low PDI (polydispersity index) values indicate the production of nanoparticles with narrow size distributions (Fig. 1), which are desirable for medical applications.

All produced lattices were stable and could be stored for months, with exception of the latex prepared with 15 wt% of AA. As observed experimentally, particle agglomeration took place in this case, leading to a latex with the largest average particle diameter and the broadest particle size distribution (Fig. 1). This may possibly be explained by the occurrence of homogeneous nucleation in the aqueous phase, as AA is completely soluble in water and can form new polymer particles through agglomeration of PAA chains [45]. Besides, the increase of the viscosity of the aqueous phase, due to accumulation of water-soluble PAA chains, can also facilitate particle agglomeration [46]. Moreover, accumulation of PAA chains on the particle surfaces can lead to formation of hairy polymer particles [47], also facilitating particle agglomeration through entanglement of soluble hydrophilic polymer segments. For these reasons, the zeta potential analysis of this sample could not be performed reliably. At lower AA concentrations (7.5 wt%, 10 wt% and 12 wt%), no significant changes of emulsion stability could be observed and small nanosized polymer particles were obtained.

Zeta potential analyses allow the evaluation of the magnitude of the accumulated surface charges, which significantly affect the stability of the dispersion [48]. According to Table 1, all particles exhibited negative zeta potentials of high magnitudes (more negative than −30 mV), indicating latex stability by electric repulsion. Negative potential values can be associated with the nature of the anionic surfactant, which tends to accumulate on the particles surface to stabilize the emulsion and prevent coalescence. Similar results were also obtained for P (MMA-co-AA) copolymerizations conducted in a previous study [39]. Particularly, comparison of zeta potentials obtained for PMMA homopolymers, PMMA-based copolymers and rivastigmine-containing nanoparticles did not indicate significant changes of size, size distributions or surface characteristics, suggesting that neither the drug nor the comonomer affected the latex stability significantly (with exception of the latex produced with 15 wt% of AA, as already discussed) and that the surfactant exerts a dominant effect on surface properties and latex stability, as also observed previously [39].

Regarding the encapsulation efficiency, and based on Table 1, higher initial rivastigmine concentrations resulted in higher encapsulation efficiencies for both homopolymer and copolymers nanoparticles. This result could already be expected because the drug is hydrophobic and tends to remain in the organic phase, so that the relative amount of drug that is dissolved in the aqueous phase is expected to decrease with the increase of the drug concentration in the organic phase. Besides, no significant differences of encapsulation efficiencies were found when the amounts of AA were increased. Particularly, 1.5 wt% of drug could be successfully encapsulated in the produced particles, which was at least three times higher than reported previously in other studies that used different techniques to encapsulate rivastigmine [15,40–43,49], which indicates the high potential of P(MMA-co-AA) nanoparticles to encapsulate rivastigmine free base.

Table 1
Average diameters, polydispersity indexes (PDI) and zeta potentials of the obtained nanoparticles.

	Size (nm)	PDI	Zeta Potential (mV)	EE% ±standard deviation
PMMA	76.64	0.229	-46.8	–
P(MMA-co-AA) 7.5%	64.55	0.216	-45.8	–
P(MMA-co-AA) 10%	81.82	0.217	-41.7	–
P(MMA-co-AA) 12%	72.42	0.216	-40.8	–
P(MMA-co-AA) 15%	536.70	1.000	ND[a]	–
PMMA+0.5%R	74.49	0.236	-45.8	81.96±3.70
P(MMA-co-AA) 10% +0.5%R	75.51	0.233	-39.4	80.68±2.68
P(MMA-co-AA) 12% +0.5%R	75.18	0.154	-40.9	73.20±1.44
PMMA +1.0%R	81.26	0.217	-52.4	91.54±2.37
P(MMA-co-AA) 10% +1.0%R	80.76	0.239	-40.3	88.92±1.18
PMMA +1.5%R	58.29	0.080	-44.3	95.78±2.04
P(MMA-co-AA) 7.5% +1.5%R	69.82	0.129	-42.9	85.68±1.13

[a] ND=not determined, due to suspension instability.

3.2. Monomer conversion

The copolymerization of AA with MMA allows the insertion of carboxylic groups onto the particle surfaces that can be used for particle functionalization in a subsequent reaction step. However, as AA is very reactive, addition of AA into the reaction medium can significantly affect the course of the polymerization and the properties of the final product.

Fig. 2-A shows the dynamic trajectories of overall monomer conversions for the distinct reactions. As shown in all cases, reactions were extremely fast and monomer conversions approached 100% in less than 20 min, indicating that polymerization reactions could be safely halted after 60 min of reaction. Additionally, monomer conversions were not very sensitive to addition of AA at the analyzed conditions. Fig. 2-B shows dynamic trajectories of overall monomer conversions when reactions were performed in the presence of the drug. As in the case of the copolymerization, addition of rivastigmine did not affect the monomer conversion trajectories significantly, as high conversion values were obtained once more in less than 20 min. This can be regarded as a very positive behavior, as previous studies reported the significant inhibitory effect of encapsulated drugs on polymerization kinetics [50–52]. Therefore, addition of rivastigmine to the reaction medium at the analyzed concentrations did not modify the course of the polymerization process, which is certainly beneficial for encapsulation proposes.

3.3. GPC analyses

Table 2 shows the average molar mass values and the polydispersities of the obtained copolymers.

As one can see in Table 2 and Fig. 3, the addition of AA tends to cause the increase of the average molar masses, possibly explained by the high reactivity of AA. On the other hand, addition of rivastigmine tends to cause the decrease of the average molar masses and the increase of the

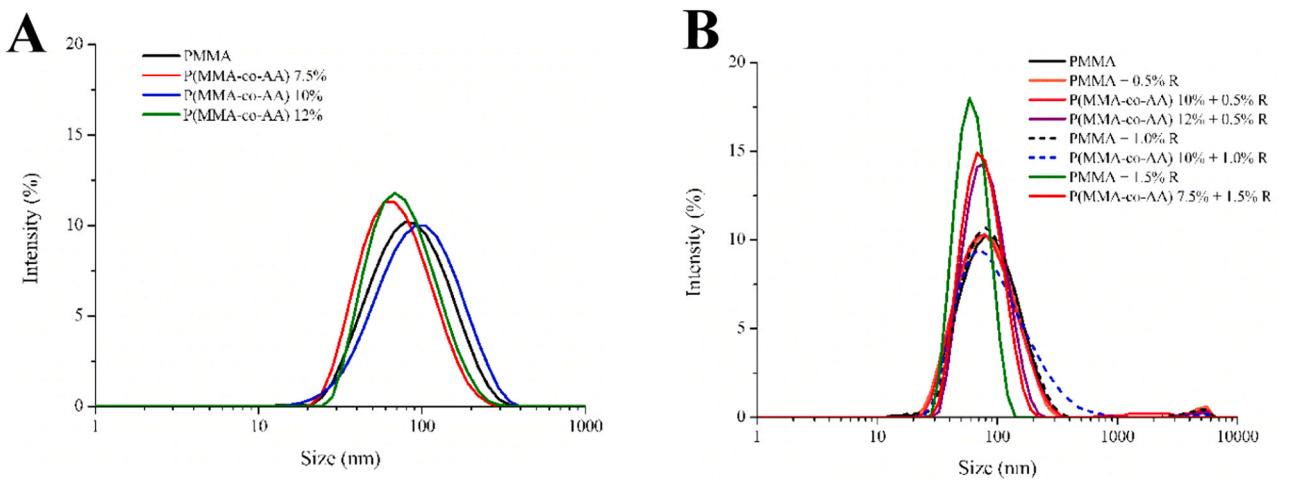

Fig. 1. Particle size distributions of obtained polymer materials in the absence (A) or in the presence (B) of rivastigmine.

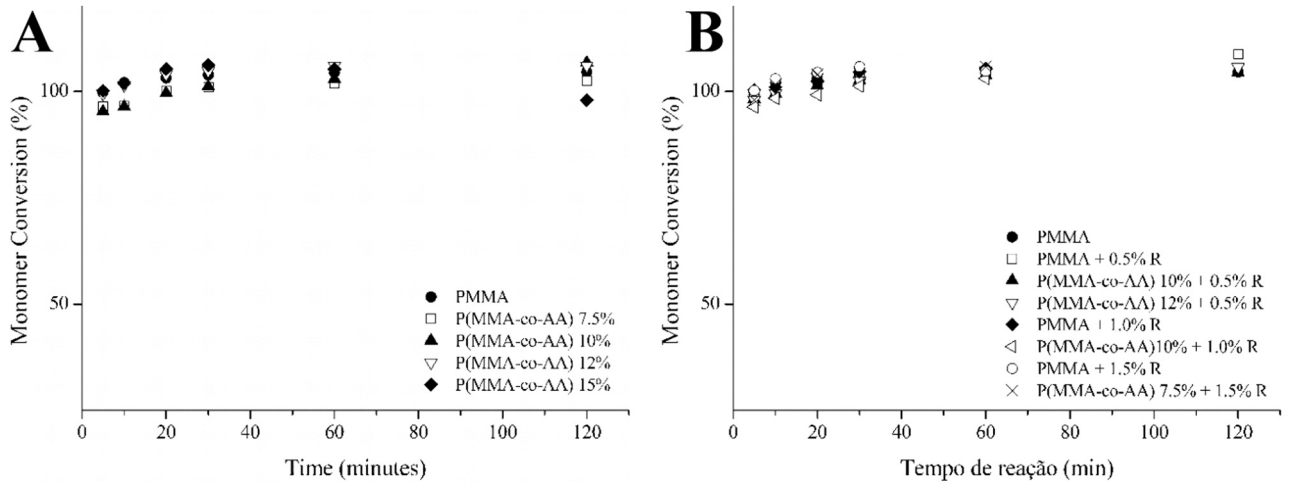

Fig. 2. Overall monomer conversion trajectories in distinct polymerization trials in the absence (A) or in the presence (B) of rivastigmine.

Table 2
Weight average molar masses (Mw) and polydispersities (PDI) of obtained polymer materials.

	Mw (kDa)	PDI
PMMA	1534	2.40
P(MMA-co-AA) 7.5%	1743	3.59
P(MMA-co-AA) 10%	2098	1.98
P(MMA-co-AA) 12%	2099	1.91
PMMA +0.5%R	1456	3.26
P(MMA-co-AA) 10% +0.5%R	1550	3.77
P(MMA-co-AA) 12% +0.5%R	1048	7.37

polydispersity index, indicating the possible role of the drug as a chain transfer agent. This chain transfer effect could be associated with the presence of multiple functional groups in the drug, corroborating the findings of previous works that detected similar effects when multifunctional drugs were added to free-radical polymerization systems [50–53].

Fig. 3-A shows that, in absence of rivastigmine, all distributions were somewhat similar. However, Fig. 3-B shows that, in presence of rivastigmine, shifting towards lower molar masses could be observed, with formation of a bimodal distribution when 12 wt% of AA were used. This reinforces the assumption that rivastigmine interacts with the reacting system as a non-ideal chain transfer agent, particularly in presence of AA molecules, shifting molar mass distributions without affecting monomer conversions considerably. Despite that, the molecular weights were always sufficiently high to assure the successful occurrence of the polymerization reaction and guarantee the mechanical integrity of the obtained particulate material.

3.4. NMR analyses

NMR analyses were performed to characterize the incorporation of the comonomer and possible structural modifications of the polymer chains produced in the presence of rivastigmine. Fig. 4 presents the NMR spectra obtained for samples of polymer products obtained in trials PMMA (A), PMMA +1.5%R (B), P(MMA-co-AA)7.5% (C) and P(MMA-co-AA)7.5% +1.5R (D).

As it might already be expected, all spectra presented the characteristic signals associated with the PMMA structure. The peak positioned at δ=3.6 ppm is related to the ester group O-CH_3 (H1 in Fig. 4), while the peaks placed at δ=1.6–2.0 ppm and δ=0.8–1.0 ppm are associated with methylene and methyl groups, respectively [54]. The peak located at δ=5.2–5.7 ppm is related to the double bond of the MMA monomer, indicating the existence of residual monomer in some final samples [54]. The copolymer compositions were calculated using the signal placed at δ=2.3–2.6 ppm (H2 in Fig. 4) [39,55], present in the copolymer material only, and were equal to 1.5 mol% for reaction P(MMA-co-AA) 12% and 1.3 mol% for reactions P(MMA-co-AA)10% (not shown) and 0.9 mol%

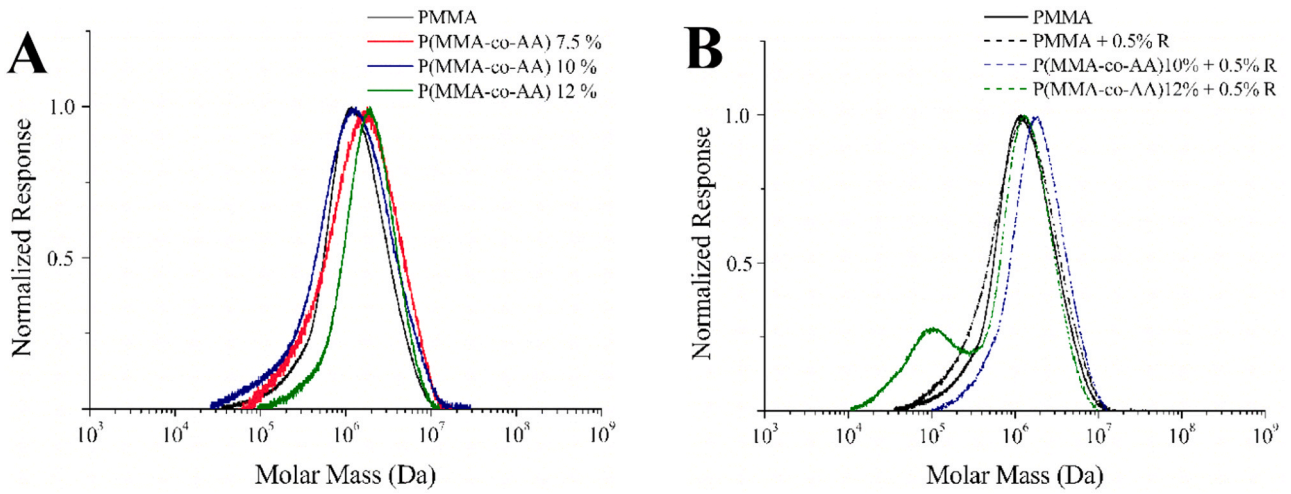

Fig. 3. Molar mass distributions of the obtained polymer materials in the absence (A) or in the presence (B) of rivastigmine.

for P(MMA-co-AA) 7.5%. These results are consistent with the ones presented by Campos, Ferraz and Pinto (2016), who explained the lower AA incorporation because of the AA polymerization in the aqueous phase, given the use of an aqueous soluble initiator (KPS). When using 1.5 wt% of rivastigmine, the copolymerization of P(MMA-co-AA) 7.5% resulted in the final AA content of 1.9 mol%, confirming that significant part of the AA remains in the aqueous phase and suggesting that the drug can possibly affect the solubility of AA in the organic phase, allowing the slight increase of AA incorporation into the polymer chains.

Regarding the presence of rivastigmine in the nanoparticles, the characteristic signals of the aromatic ring present in the drug (Fig. 4) at δ=7.03 ppm and δ=7.31 ppm were not present in the obtained NMR spectra of the encapsulated materials (Figs. 4-B and D). However, the NMR spectra revealed the presence of rivastigmine in 50:50 physical mixtures with polymer samples (see Fig. 4-E). This shows that rivastigmine can be indeed observed through NMR H^1 analyses and reinforces that the absence of the characteristic signals of rivastigmine in the nanoparticle samples is probably due to the low drug contents, given the high encapsulation efficiencies shown in Table 1.

3.5. FT-IR analyses and functionalization

FT-IR analyses confirmed that addition of rivastigmine did not cause any significant modification of the obtained polymer material, as reinforced by the high linear correlation coefficients of FT-IR spectra of the different materials shown in Fig. 5.

According to Fig. 5-A, the peaks positioned at 2900 cm^{-1}, 1720 cm^{-1} and 1100 cm^{-1} can be attributed to the chemical bounds O-H, C-O-C e C=O of carboxylic and ester groups present in both homopolymers and copolymers [39,56,57]. Bands placed at 1475–1600 cm^{-1} that could be associated with the aromatic rings of the drug were not found, due to the low drug concentrations and successful encapsulation of drug molecules.

Fig. 5-B presents the linear correlations of FT-IR spectra of materials prepared in absence and presence of rivastigmine. The high correlation coefficients (R^2>0.9) indicate the high similarity of the analyzed samples and the small influence of rivastigmine on the chemical nature of the final polymer. Nevertheless, one can observe that the linear correlation is somewhat lower when AA was added to the reaction system, reinforcing the assumption that rivastigmine interacts preferentially with AA molecules, as observed previously through the molar mass distributions.

It is important to note that the peaks placed at 1600 cm^{-1} and 1640 cm^{-1} shown in Fig. 5-C could only be detected for functionalized nanoparticles, indicating the successful formation of chemical links between the nanoparticle support and the bioactive immobilized TAT and lysine molecules. This band was less intense for TAT-containing products than for lysine-containing materials, which can be associated with the much smaller size of lysine molecules and consequently more frequent formation of chemical bonds on the surfaces of the nanoparticles in this case. Also, the presence of rivastigmine did not affect the functionalization process, as the band placed at 1600 cm^{-1} could be observed in presence or absence of the drug. Particularly, the peaks positioned at 3100–3300 cm^{-1} and 1600–1700 cm^{-1} are characteristic of the amino groups present in both TAT and lysine molecules [39,57], confirming the successful functionalization of the final nanoparticles.

It is important to remark that functionalization did not cause any significant change of the physicochemical properties of the obtained nanoparticles, as shown in Table 3. Lysine functionalized particles presented diameters that were approximately 25 nm larger than observed for original particles and kept the narrow size distributions (PDI<0.1). This was also true for the TAT immobilized nanoparticle selected for *in vitro* studies: PMMA-co-AA 7.5% +1.5%R. These measurements are in agreement with previous surface corona studies that indicated the approximate increment of 30 nm in average diameters of nanoparticles conjugated with multiple biomolecules [58]. However, an exception was observed for P(MMA-co-AA) 12%, which showed a substantial increase of the z-average diameter. The higher hydrodynamic diameter could possibly suggest a physical multilayer sorption of lysine in addition to the chemical functionalization. Insignificant variation of the zeta potentials values was noticed in all cases, indicating the strong influence of the anionic surfactant on this property.

3.6. Evaluation of cytotoxicity and cell permeability of Caco-2 cells

The assessment of the toxicity and characterization of possible biological interactions can be of fundamental importance for use of nanoparticles as drug delivery materials. For this reason, cultures of Caco-2 cells were selected as appropriate *in vitro* model due to the intrinsic capacity of these cells to form tight junctions and confluent cell monolayers, as in the case of BBB cells, being for this matter widely used an accurate model for cell transport studies [59]. Particularly, Caco-2 cells allow the evaluation of the toxicity of rivastigmine-loaded nanoparticles and their ability to permeate trough complex biological barriers.

It is important to mention that the free reference drug showed no cytotoxicity effect (CC_{50}>250 μg/mL, Table 4) on Caco-2 cells, which was already expected, given previous findings of acute toxicity of rivastigmine in epithelial cells only when concentrations reached 50 mg/mL [60]. Scialabba et al. (2012) also reported low toxicity of rivastigmine in neuroblastoma cells treated with maximum concentration of 0.2 mg/mL, which is a much higher concentration value than the ones

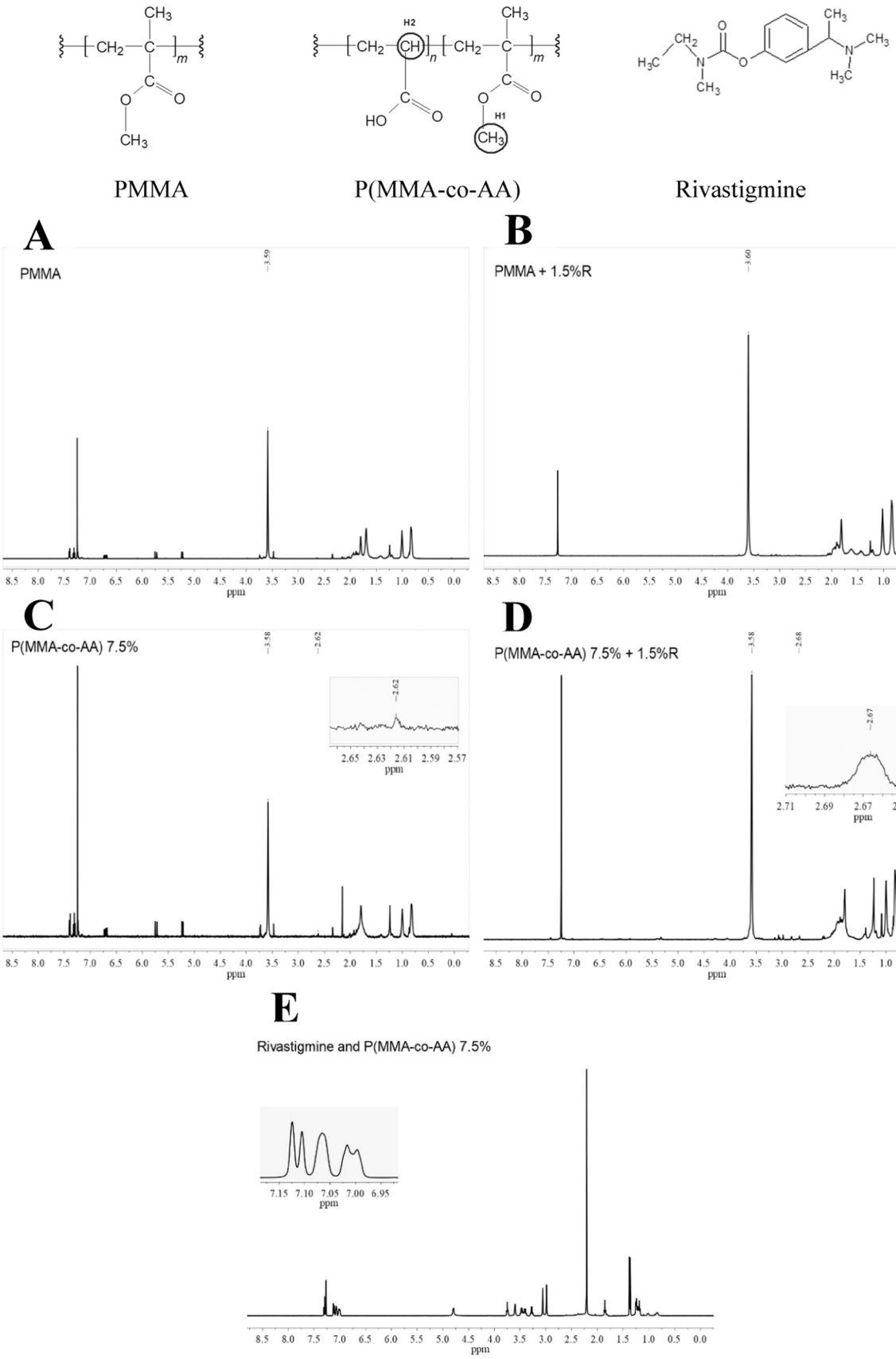

Fig. 4. Chemical structures of the analyzed (co)polymers and drug and ^{1}H NMR spectra of the obtained nanomaterials in the absence (A, C), in the presence (B, D) and in the 50:50 physical mixture with rivastigmine (E).

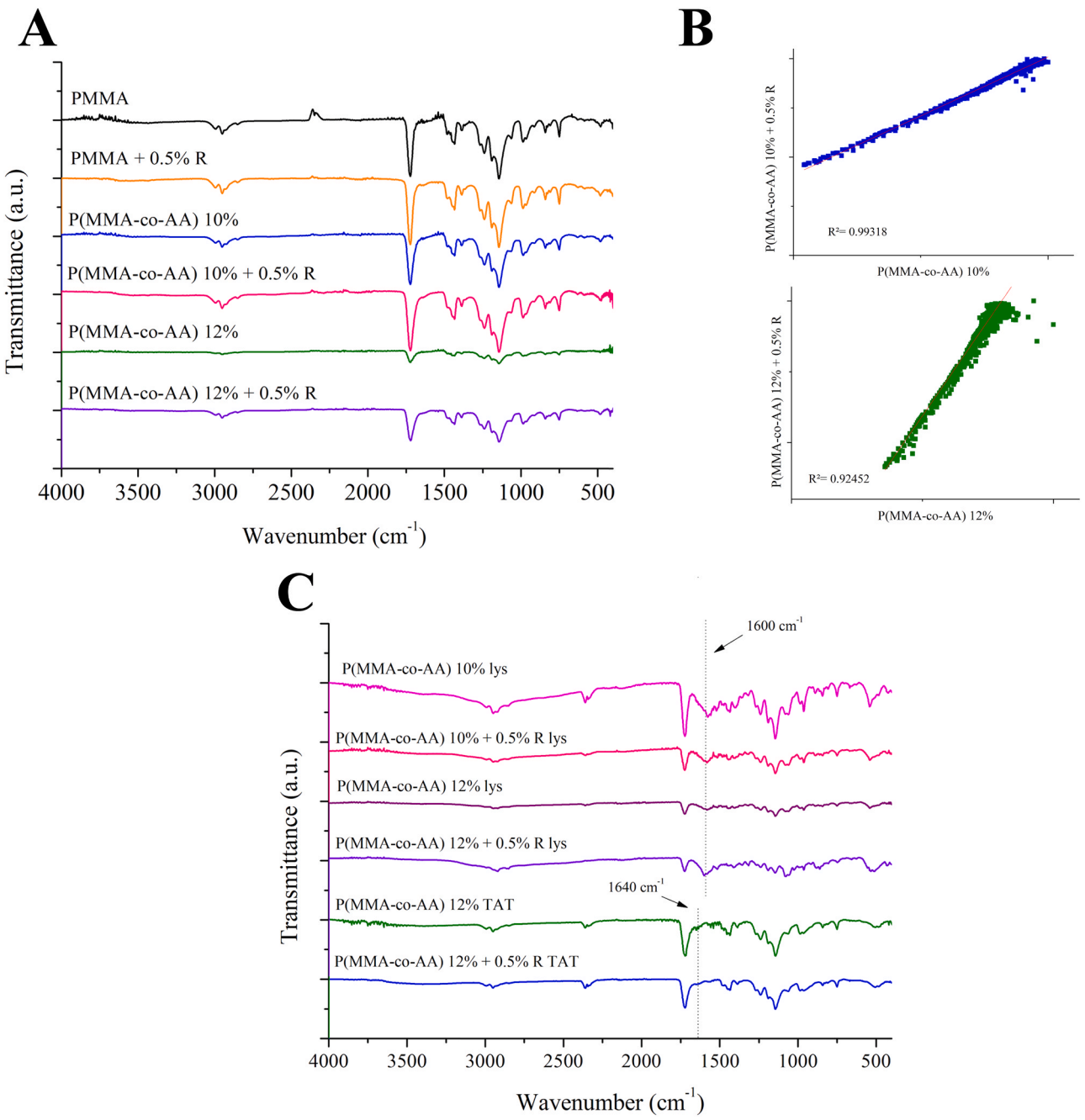

Fig. 5. FT-IR spectra of the obtained polymer materials (A), the linear correlation of spectra obtained and the presence and absence of rivastigmine (B), and the spectra of the functionalized materials (C).

Table 3
Average diameters, polydispersity indexes (PDI) and zeta potentials of the functionalized nanoparticles.

	Size (nm)	PDI	Zeta potential (mV)
P(MMA-co-AA) 7.5% +LIS	86.54	0.051	- 38.2
P(MMA-co-AA) 10% +LIS	107.73	0.070	- 39.9
P(MMA-co-AA) 12% +LIS	138.93	0.089	- 41.4
P(MMA-co-AA) 7.5% +1.5%R +TAT	73.38	0.079	- 42.1

Table 4
Cytotoxic effect of the nanoparticles on Caco-2 cells.

CC_{50} (μg/mL rivastigmine)±standard deviation	
Free rivastigmine (R)	>250
PMMA	52.31±7.46
P(MMA-co-AA) 7.5%	34.52±10.80
PMMA +1.5%R	52.86±9.28
P(MMA-co-AA) 7.5% +1.5%R	51.26±16.76

tested here. Nevertheless, the nanoparticles prepared in presence or absence of the drug reached CC_{50} value of approximately 52 μg/mL (Table 4), suggesting that the cytotoxic effect can be attributed to the latex components, such as the surfactant, but not to the polymer material. Additionally, the cytotoxic effects of both homopolymer (PMMA; CC_{50}=52.31±7.46 μg/mL) and copolymer (PMMA-co-AA; CC_{50}=34.52±10.80 μg/mL) materials were very similar to the cytotoxic effects of drug-loaded nanoparticles (Table 4). However, toxicity does

not seem to be associated with the comonomers, as the selected comonomers have been widely used for manufacture of many distinct materials intended for biomedical applications [61]. As a matter of fact, the obtained data suggest that the nanoparticle toxic effect can be associated with the ingredients of the latex, such as the surfactant (SDS) present in the reaction and in the final latex formulation. This hypothesis is strongly supported by the continuing discussion regarding the cellular toxicity of surfactants in general and of SDS in particular [62,63], which drives the continuous search for more biocompatible surfactants for these polymerization systems [64].

Nevertheless, it is important to highlight that the encountered CC_{50} values are associated with large periods of incubation (72 h) and high concentrations of nanoparticles (1.4 mg/mL), which are indeed too high when compared to expected real *in vivo* applications, given the low amounts of rivastigmine recommended for medical treatment. Additionally, previous reports indicated low toxic effect of poly(methacrylated α,β-poly(N-2-hydroxyethyl)-dl-aspartamide) (PHM) nanoparticles (1 mg/mL) in human myeloid leukemia cells (K-562) [44] and of PMMA nanoparticles (1 mg/mL) in human leukemic cells (THP1) and pulmonary adenocarcinoma (A549) [28]. It is also important to indicate that freeze dried PMMA nanoparticles synthesized with similar methodology and using SDS as surfactant were also tested in K-562 cells and showed no significant toxicity up to 1.5 mg/mL of nanoparticles [65], which once more shows the impact of the composition of the latex suspension on the cytotoxicity and the safe use of PMMA nanoparticles.

Pharmacokinetic studies conducted with AD patients using capsules and patches of rivastigmine showed a maximum plasma concentration of 21.6 ng/mL of the drug with a top absorption rate of 8.1 h [66]. When comparing these results with the CC_{50} values obtained here, it can be easily noted that the CC_{50} is 2,400 times higher than the maximum drug plasma concentration reported in human clinical treatment. Therefore, the required nanoparticle concentration needed for treatment would hardly reach toxic effects, ensuring a good safety profile of the synthesized drug carriers.

Regarding the permeability assays, the transport of nanoparticles through EDTA treated Caco-2 cells, taken as positive control as it can alter tight junctions (Fig. 6), were statistically similar (±25%) to the permeability of all the tested nanoparticle formulations (Table 5). This indicates that, for the analyzed time course of 4 h, the nanoparticles could successfully permeate through biological barriers independently of functionalization. The confirmation of cellular junction integrity (Fig. 6) showed that the nanoparticles did not induce cytotoxic effects, as tight junction disruption, maintaining the selectivity and transepithelial electrical resistance of Caco-2 cells. The obtained fluorescence images reinforce that the transport of nanoparticles was performed only through the cell membrane (Fig. 6). Loss of tight junction integrity was clearly observed only in EDTA treated Caco-2 cells (Fig. 6). Thus, the obtained data suggest that all the analyzed nanoparticles presented high permeation ability through the membranes, since only 4 h were sufficient to ensure the fast passage until gradient equity, which constitutes a very positive result. Also, the observed permeability values were very similar to the positive control (without addition of Caco-2 cells), indicating that the nanoparticles permeated without extra resistance through the monolayer of intestinal epithelial cells.

Similar performances of functionalized and non-functionalized nanocarriers were also reported by Yang et al. (2013) for *in vitro* permeation of CPP-functionalized liposomes loaded with rivastigmine through endothelial cells of mice for 24 h [67]. Thus, nanoparticle internalization can be achieved without the aid of TAT, which can be attributed to the reduced size of the nanoparticles. Feng et al. (2005) showed that cellular uptake of polymeric nanoparticles by Caco-2 can be significantly affected by the polymer material, concentration (500 μg/mL showed the best results) and size (with optimum uptake with 100 nm nanoparticles), indicating the existence of a very complex

Table 5
Nanoparticles permeability in Caco-2 cells.

Cellular Permeability (%) ±standard deviation	
EDTA Treated Cells	24.40±0.92
P(MMA-co-AA) 7.5%	27.10±2.13
P(MMA-co-AA) 7.5% +TAT	23.64±0.27
P(MMA-co-AA) 7.5% +1.5%R	24.05±0.03
P(MMA-co-AA) 7.5% +1.5%R +TAT	23.60±1.32

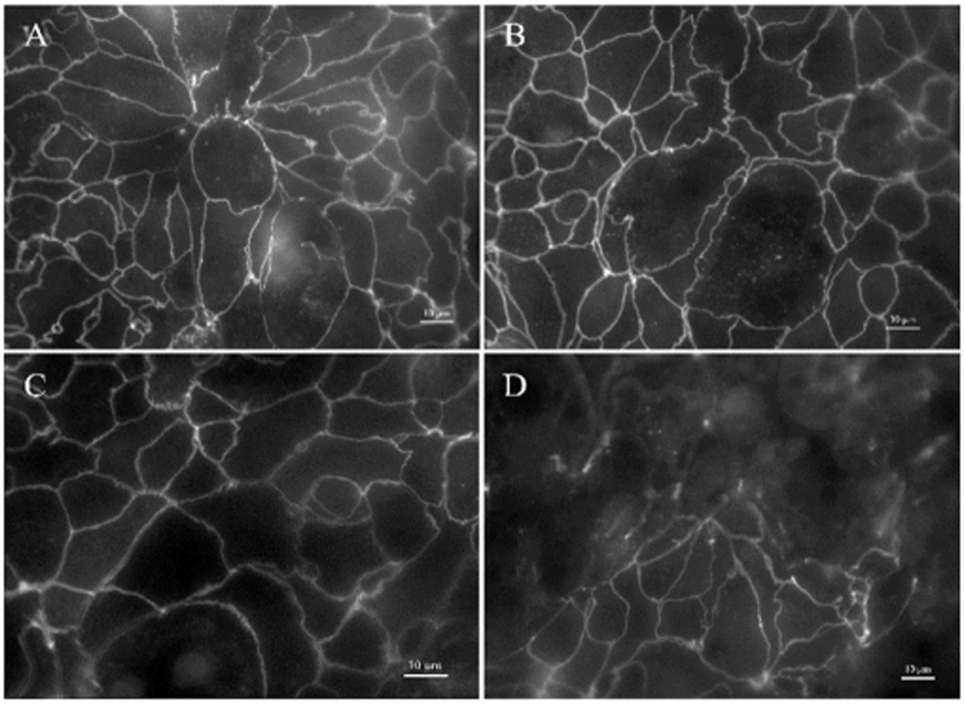

Fig. 6. Micrographs obtained after performing the Transwell test for cell control (A), test with P (MMA-co-AA) 7.5% (B), P (MMA-co-AA) 7.5% +1.5%R (C) and positive control (D).

process that involves a combination of many nanomaterials properties. Interestingly, the authors observed a plateau of cellular uptake that indicates the occurrence of saturation values for nanoparticle concentration and time of incubation (from 2 h) [68]. The latter could possibly explain the results found here, since the similar performances of functionalized and non-functionalized nanoparticles could be associated with this plateau due to the long incubation periods. Mechanistic studies conducted with Caco-2 cells and polymeric nanoparticles (of 100 nm) indicated the existence of non-specific transport mechanisms with high permeation capacity, as fast as 1 h [69], reinforcing that the long experiments can explain the observed cellular uptake of functionalized and non-functionalized nanoparticles. Taken together, these results indicate the fast permeation capacity of the synthesized nanoparticles and suggest that other variables can be manipulated to characterize the phenomena that can control the passage of the studied nanodevices through physiological barriers.

4. Conclusion

The present study investigated the encapsulation of rivastigmine in poly(methyl methacrylate – co – acrylic acid), P(MMA-co-AA), nanoparticles functionalized with the transcription activator peptide (TAT) and intended for biomedical applications. Encapsulation was performed *in situ* through miniemulsion polymerization at different preparation conditions, leading to nanoparticles with average diameters below 100 nm and with narrow size distributions. Particularly, the highest encapsulation efficiencies (around 80%) were obtained when the comonomer mixture contained 7.5 wt% of acrylic acid in methyl methacrylate. Moreover, it was shown that although the drug interacts with the reaction medium, leading to a lower molar mass distribution, its copolymerization was not observed. Morphological and functionalization features of the nanoparticles were not affected by the drug.

Functionalization of polymer nanoparticles was performed through chemical adsorption, leading to high TAT immobilization efficiencies (94%). Additionally, toxicity bioassays conducted with Caco-2 cells monolayers revealed that the cytotoxicity of obtained particles was low (CC_{50} above 50 μg/mL of rivastigmine or 1.4 mg/mL of nanoparticles) and did not depend on the nanoparticle composition. Besides, the obtained results indicated that the functionalized nanoparticles could cross the intestinal epithelial barrier successfully without damaging the cellular tight junctions. Finally, the obtained particles presented good stability, could be prepared with high encapsulation and functionalization efficiencies, and presented advantageous biological properties that encourage the future development of biomedical uses.

CRediT authorship contribution statement

Mangia L.H.R.: Conceptualization, Methodology, Validation, Investigation, Writing, Visualization. **Ferraz H.C.:** Conceptualization, Methodology, Supervision, Writing, Project administration, Funding. **Souza R.S.D.:** Investigation, Resources. **Pereira M.C.S.:** Investigation, Resources, Writing. **Pinto J.C.:** Conceptualization, Methodology, Supervision, Writing, Project administration, Funding.

Declaration of Competing Interest

The authors declare that they have no known competing financial interests or personal relationships that could have appeared to influence the work reported in this paper.

Acknowledgments

The authors thank Conselho Nacional de Desenvolvimento Científico e Tecnológico, Brazil (CNPq), Coordenação de Aperfeiçoamento de Pessoal de Nível Superior, Brazil (CAPES) and Fundação Carlos Chagas Filho de Amparo à Pesquisa do Estado do Rio de Janeiro, Brazil (FAPERJ) for supporting this work and providing scholarships.

References

[1] R. Anand, K.D. Gill, A.A. Mahdi, Therapeutics of Alzheimer's disease: past, present and future, Neuropharmacology 76 (2014) 27–50, https://doi.org/10.1016/j.neuropharm.2013.07.004.
[2] R.S. Wilson, E. Segawa, P.A. Boyle, S.E. Anagnos, L.P. Hizel, D.A. Bennett, The natural history of cognitive decline in Alzheimer's disease, Psychol. Aging 27 (2012) 1008–1017, https://doi.org/10.IO37/aOO29857.
[3] R.A. Hickman, A. Faustin, T. Wisniewski, Alzheimer disease and its growing epidemic: risk factors, biomarkers, and the urgent need for therapeutics, Neurol. Clin. 34 (2016) 941–953, https://doi.org/10.1016/j.ncl.2016.06.009.
[4] K. Mullane, M. Williams, Alzheimer's therapeutics: continued clinical failures question the validity of the amyloid hypothesis - but what lies beyond? Biochem. Pharmacol. 85 (2013) 289–305, https://doi.org/10.1016/j.bcp.2012.11.014.
[5] A. Kumar, A. Singh, Ekavali, A review on Alzheimer's disease pathophysiology and its management: an update, Pharmacol. Rep. 67 (2015) 195–203, https://doi.org/10.1016/j.pharep.2014.09.004.
[6] L.E. Hebert, J. Weuve, P.A. Scherr, L.E. Hebert, J. Weuve, Alzheimer disease in the United States (2010–2050) estimated using the 2010 census, Neurology 80 (2013) 1778–1783, https://doi.org/10.1212/WNL.0b013e31828726f5.
[7] Alzheimer's Association, 2019 Alzheimer's disease facts and figures, Alzheimer's Dement. 15 (2019) 321–387, https://www.alz.org/media/Documents/alzheimers-facts-and-figures-2019-r.pdf.
[8] B. Eftekharzadeh, B.T. Hyman, S. Wegmann, Structural studies on the mechanism of protein aggregation in age related neurodegenerative diseases, Mech. Ageing Dev. 156 (2016) 1–13, https://doi.org/10.1016/j.mad.2016.03.001.
[9] D. Galimberti, E. Scarpini, Treatment of Alzheimer's Disease: Symptomatic and Disease-Modifying Approaches, 2010, pp. 46–56. ⟨https://doi.org/10.2174/156720510790274400⟩.
[10] K.G. Yiannopoulou, S.G. Papageorgiou, Current and future treatments for Alzheimer's disease, Ther. Adv. Neurol. Disord. 6 (2013) 19–33, https://doi.org/10.1177/1756285612461679.
[11] R. Annicchiarico, A. Federici, C. Pettenati, C. Caltagirone, Rivastigmine in Alzheimer's disease: cognitive function and quality of life, Ther. Clin. Risk Manag. 3 (2007) 1113–1123.
[12] T. Muller, Rivastigmine in the treatment of patients with Alzheimer's disease, Neuropsychiatr. Dis. Treat. 3 (2007) 211–218.
[13] R.A. Hansen, G. Gartlehner, A.P. Webb, L.C. Morgan, C.G. Moore, D.E. Jonas, Efficacy and safety of donepezil, galantamine, and rivastigmine for the treatment of Alzheimer's disease: a systematic review and meta-analysis, Clin. Interv. Aging 3 (2008) 211–225.
[14] B. Fonseca-Santos, M. Chorilli, M. Palmira Daflon Gremião, Nanotechnology-based drug delivery systems for the treatment of Alzheimer's disease, Int. J. Nanomed. 10 (2015) 4981–5003, https://doi.org/10.2147/IJN.S87148.
[15] S.A. Joshi, S.S. Chavhan, K.K. Sawant, Rivastigmine-loaded PLGA and PBCA nanoparticles: preparation, optimization, characterization, in vitro and pharmacodynamic studies, Eur. J. Pharm. Biopharm. 76 (2010) 189–199, https://doi.org/10.1016/j.ejpb.2010.07.007.
[16] J. Kreuter, Drug delivery to the central nervous system by polymeric nanoparticles: what do we know? Adv. Drug Deliv. Rev. 71 (2014) 2–14, https://doi.org/10.1016/j.addr.2013.08.008.
[17] K. Nagpal, S.K. Singh, D.N. Mishra, Optimization of brain targeted chitosan nanoparticles of Rivastigmine for improved efficacy and safety, Int. J. Biol. Macromol. 59 (2013) 72–83, https://doi.org/10.1016/j.ijbiomac.2013.04.024.
[18] R.A. Siegel, M.J. Rathbone, Overview of controlled release mechanisms, in: J. Siepmann, R.A. Siegel, M.J. Rathbone (Eds.), Fundamentals and Applications of Controlled Release Drug Delivery, Springer US, Boston, MA, 2012, pp. 19–43, https://doi.org/10.1007/978-1-4614-0881-9_2.
[19] K. Park, Controlled drug delivery systems: past forward and future back, J. Control. Release 190 (2014) 3–8, https://doi.org/10.1016/j.jconrel.2014.03.054.
[20] M. Elsabahy, K.L. Wooley, Design of polymeric nanoparticles for biomedical delivery applications, Chem. Soc. Rev. 41 (2012) 2545–2561, https://doi.org/10.1039/c2cs15327k.
[21] C. Saraiva, C. Praça, R. Ferreira, T. Santos, L. Ferreira, L. Bernardino, Nanoparticle-mediated brain drug delivery: overcoming blood–brain barrier to treat neurodegenerative diseases, J. Control. Release 235 (2016) 34–47, https://doi.org/10.1016/j.jconrel.2016.05.044.
[22] Y. Chen, L. Liu, Modern methods for delivery of drugs across the blood–brain barrier, Adv. Drug Deliv. Rev. 64 (2012) 640–665, https://doi.org/10.1016/j.addr.2011.11.010.
[23] J. Kreuter, Nanoparticulate systems for brain delivery of drugs, Adv. Drug Deliv. Rev. 47 (2001) 65–81, https://doi.org/10.1016/j.addr.2012.09.015.
[24] J.R. Kanwar, X. Sun, V. Punj, B. Sriramoju, R.R. Mohan, S.-F. Zhou, A. Chauhan, R. K. Kanwar, Nanoparticles in the treatment and diagnosis of neurological disorders: untamed dragon with fire power to heal, Nanomed. Nanotechnol. Biol. Med 8 (2012) 399–414, https://doi.org/10.1016/j.nano.2011.08.006.
[25] K. Ulbrich, T. Hekmatara, E. Herbert, J. Kreuter, Transferrin- and transferrin-receptor-antibody-modified nanoparticles enable drug delivery across the blood–brain barrier (BBB), Eur. J. Pharm. Biopharm. 71 (2009) 251–256, https://doi.org/10.1016/j.ejpb.2008.08.021.
[26] L.-L. Zou, J.-L. Ma, T. Wang, T.-B. Yang, C.-B. Liu, Cell-penetrating peptide-mediated therapeutic molecule delivery into the central nervous system, Curr.

Neuropharmacol. 11 (2013) 197–208, https://doi.org/10.2174/1570159×11311020006.
[27] K.S. Rao, M.K. Reddy, J.L. Horning, V. Labhasetwar, TAT-conjugated nanoparticles for the CNS delivery of anti-HIV drugs, Biomaterials 29 (2008) 4429–4438, https://doi.org/10.1016/j.biomaterials.2008.08.004.
[28] P.E. Feuser, P.C. Gaspar, E. Ricci-Júnior, M.C.S. da Silva, M. Nele, C. Sayer, P.H. H. de Araújo, Synthesis and characterization of poly(methyl methacrylate) PMMA and evaluation of cytotoxicity for biomedical application, Macromol. Symp. 343 (2014) 65–69, https://doi.org/10.1002/masy.201300194.
[29] S.S. Halacheva, D.J. Adlam, E.K. Hendow, T.J. Freemont, J. Hoyland, B. R. Saunders, Injectable biocompatible and biodegradable ph-responsive hollow particle gels containing poly(acrylic acid): the effect of copolymer composition on gel properties, Biomacromolecules 15 (2014) 1814–1827, https://doi.org/10.1021/bm5002069.
[30] G. Dai, Q. Xie, S. Chen, C. Ma, G. Zhang, Biodegradable poly(ester)-poly(methyl methacrylate) copolymer for marine anti-biofouling, Prog. Org. Coat. 124 (2018) 55–60, https://doi.org/10.1016/j.porgcoat.2018.08.003.
[31] J.A. Méndez, G.A. Abraham, M.D.M. Fernández, B. Vázquez, J.S. Román, Self-curing acrylic formulations containing PMMA/PCL composites: properties and antibiotic release behavior, J. Biomed. Mater. Res. 61 (2002) 66–74, https://doi.org/10.1002/jbm.10142.
[32] Z. Jing, A. Xu, Y. Liang, Z. Zhang, C. Yu, P. Hong, Y. Li, Biodegradable poly(acrylic acid-co-acrylamide)/poly(vinyl alcohol) double network hydrogels with tunable mechanics and high self-healing performance, Polymers (Basel) 11 (2019) 952, https://doi.org/10.3390/polym11060952.
[33] C.K. Weiss, K. Landfester, Miniemulsion polymerization as a means to encapsulate organic and inorganic materials, in: A.M. van Herk, K. Landfester (Eds.), Advances in Polymer Science, Springer, Berlin, Heidelberg, 2010, pp. 185–236, https://doi.org/10.1007/12_2010_61.
[34] K. Landfester, C.K. Weiss, Encapsulation by miniemulsion polymerization, in: F. Caruso (Ed.), Advances in Polymer Science, Springer, Berlin, Heidelberg, 2010, pp. 1–49, https://doi.org/10.1007/12_2009_43.
[35] A. Gharieh, S. Khoee, A.R. Mahdavian, Emulsion and miniemulsion techniques in preparation of polymer nanoparticles with versatile characteristics, Adv. Colloid Interface Sci. 269 (2019) 152–186, https://doi.org/10.1016/j.cis.2019.04.010.
[36] G.T. Hermanson, Microparticles and nanoparticles, in: G.T. Hermanson (Ed.), Bioconjugate Chemistry, 2nd ed., Elsevier Inc, 2008, pp. 582–626, https://doi.org/10.1016/B978-0-12-370501-3.X0001-X.
[37] M. Roth, Fluorescence reaction for amino acids, Anal. Chem. 43 (1971) 880–882, https://doi.org/10.1021/ac60302a020.
[38] M.M. Bradford, A rapid and sensitive method for the quantitation microgram quantities of protein utilizing the principle of protein-dye binding, Anal. Chem. 72 (1976) 248–254, https://doi.org/10.1016/0003-2697(76)90527-3.
[39] I.M.F. Campos, H.C. Ferraz, J.C. Pinto, Production and functionalization of P (MMA-co-AA) nanoparticles by miniemulsion polymerization, Macromol. Symp. 368 (2016) 70–77, https://doi.org/10.1002/masy.201600029.
[40] S.P. Kaur, R. Rao, A. Hussain, S. Khatkar, Preparation and characterization of rivastigmine loaded chitosan nanoparticles, J. Pharm. Sci. Res. 3 (2011) 1227–1232.
[41] M. Fazil, S. Md, S. Haque, M. Kumar, S. Baboota, J.K. Sahni, J. Ali, Development and evaluation of rivastigmine loaded chitosan nanoparticles for brain targeting, Eur. J. Pharm. Sci. 47 (2012) 6–15, https://doi.org/10.1016/j.ejps.2012.04.013.
[42] K. Pagar, V. Pradeep, Rivastigmine loaded L-lactide-depsipeptide polymeric nanoparticles: decisive formulation variables optimization, Sci. Pharm. 81 (2013) 865–885, https://doi.org/10.3797/scipharm.1211-20.
[43] O. Vijaykumar, V.F. Joe, B.A. Vishwanath, Formulation and evaluation of rivastigmine loaded polymeric nanoparticles, J. Chem. Pharm. Res. 6 (2014) 556–565.
[44] E.F. Craparo, G. Pitarresi, M.L. Bondì, M.P. Casaletto, M. Licciardi, G. Giammona, A nanoparticulate drug-delivery system for rivastigmine: physico-chemical and in vitro biological characterization, Macromol. Biosci. 8 (2008) 247–259, https://doi.org/10.1002/mabi.200700165.
[45] A.C.B. Peixoto, I.M.F. Campos, H.C. Ferraz, J.C. Pinto, Use of hydrophilic monomers to avoid secondary particle nucleation in miniemulsion polymerizations of methyl methacrylate, J. Res. Updates Polym. Sci. 5 (2016) 60–71.
[46] M.-C. Chevrel, N. Brun, S. Hoppe, D. Meimaroglou, L. Falk, D. Chapron, P. Bourson, A. Durand, In situ monitoring of acrylic acid polymerization in aqueous solution using rheo-Raman technique. Experimental investigation and theoretical modelling, Chem. Eng. Sci. 106 (2014) 242–252, https://doi.org/10.1016/j.ces.2013.11.039.
[47] A. Kirillova, G. Stoychev, L. Ionov, A. Synytska, Self-assembly behavior of hairy colloidal particles with different architectures: mixed versus janus, Langmuir 30 (2014) 12765–12774, https://doi.org/10.1021/la503455h.
[48] S. Bhattacharjee, DLS and zeta potential - what they are and what they are not? J. Control. Release 235 (2016) 337–351, https://doi.org/10.1016/j.jconrel.2016.06.017.
[49] W. Barnabas, Drug targeting strategies into the brain for treating neurological diseases, J. Neurosci. Methods 311 (2019) 133–146, https://doi.org/10.1016/j.jneumeth.2018.10.015.
[50] M.A.M. Oliveira, P.A. Melo, M. Nele, J.C. Pinto, In-Situ incorporation of amoxicillin in pva/pvac-co-pmma particles during suspension polymerizations, Macromol. Symp. 299–300 (2011) 34–40, https://doi.org/10.1002/masy.200900144.
[51] M.A.M. Oliveira, P.A. Melo, M. Nele, J.C. Pinto, Suspension copolymerization of vinyl acetate and methyl methacrylate in the presence of amoxicillin, Macromol. React. Eng. 6 (2012) 280–292, https://doi.org/10.1002/mren.201100083.
[52] M.A.M. Oliveira, P.A. Melo, M. Nele, J.C. Pinto, In situ incorporation of doxorubicin in copolymer particles during suspension polymerization, Macromol. Symp. 319 (2012) 23–33, https://doi.org/10.1002/masy.201100249.
[53] L.B. Fonseca, M. Nele, N.M. Volpato, R.C. Seiceira, J.C. Pinto, Production of PMMA nanoparticles loaded with praziquantel through "'in situ"' miniemulsion polymerization, Macromol. React. Eng. 7 (2013) 54–63, https://doi.org/10.1002/mren.201200036.
[54] M. Kostrzewska, B. Ma, I. Javakhishvili, J.H. Hansen, S. Hvilsted, A.L. Skov, Controlled release in hard to access places by poly(methyl methacrylate) microcapsules triggered by gamma irradiation, Polym. Adv. Technol. 26 (2015) 1059–1064, https://doi.org/10.1002/pat.3532.
[55] D.V. Way, R.S. Braido, S.A. dos Reis, F.A. Lara, J.C. Pinto, Miniemulsion RAFT copolymerization of MMA with acrylic acid and methacrylic acid and bioconjugation with BSA, Nanomaterials (Basel, Switzerland) 9 (2019) 828, https://doi.org/10.3390/nano9060828.
[56] M.A.F. César-Oliveira, S. Zaioncz, A.R.S. Oliveira, M.C.R. Almeida, S.F. Zawadzki, L. Akcelrud, M. Aguiar, D. Tabak, Síntese de copolímeros metacrílicos através da modificação química do poli (metacrilato de metila) de massa molar controlada, Polímeros 9 (1999) 156–162.
[57] C.M.R. Ribeiro, N.A. de Souza, Esquema geral para elucidação de substâncias orgânicas usando métodos espectroscópico e espectrométrico, Quim. Nova 30 (2007) 1026–1031.
[58] C.D. Walkey, J.B. Olsen, F. Song, R. Liu, H. Guo, D.W.H. Olsen, Y. Cohen, A. Emili, W.C.W. Chan, Protein corona fingerprinting predicts the cellular interaction of gold and silver nanoparticles, ACS Nano 8 (2014) 2439–2455, https://doi.org/10.1021/nn406018q.
[59] C.F. Jones, D.W. Grainger, In vitro assessments of nanomaterial toxicity, Adv. Drug Deliv. Rev. 61 (2009) 438–456, https://doi.org/10.1016/j.addr.2009.03.005.
[60] D. Goldblum, M. Gygax, M. Böhnke, J.G. Garweg, In vitro toxicity of rivastigmine and donepezil in cells of epithelial origin, Ophthalmic Res. 34 (2002) 97–103, https://doi.org/10.1159/000048336.
[61] S.K. Swain, K. Prusty, Biomedical applications of acrylic-based nanohydrogels, J. Mater. Sci. 53 (2018) 2303–2325, https://doi.org/10.1007/s10853-017-1726-x.
[62] C. Colombo, M. Lupi, P. Ubezio, D. Moscatelli, Cytotoxicity of PMMA-based nanoparticles synthesized adopting SDS and TWEEN 80, Macromol. Symp. 324 (2013) 134–139, https://doi.org/10.1002/masy.201200078.
[63] G. Mahadevan, S. Valiyaveettil, Understanding the interactions of poly(methyl methacrylate) and poly(vinyl chloride) nanoparticles with BHK-21 cell line, Sci. Rep. 11 (2021) 2089, https://doi.org/10.1038/s41598-020-80708-0.
[64] J.B. Alves, L.H.R. Mangia, A. de, J. Sousa-Batista, H.C. Ferraz, J.C. Pinto, Effects of different stabilizers on miniemulsion methyl methacrylate polymerizations, Macromol. Symp. 394 (2020) 1–10, https://doi.org/10.1002/masy.202000143.
[65] A.N. Mendes, I. Hubber, M. Siqueira, G.M. Barbosa, D. de Lima Moreira, C. Holandino, J.C. Pinto, M. Nele, Preparation and cytotoxicity of poly(Methyl Methacrylate) nanoparticles for drug encapsulation, Macromol. Symp. 319 (2012) 34–40, https://doi.org/10.1002/masy.201100248.
[66] A. Kurz, M. Farlow, G. Lefèvre, Pharmacokinetics of a novel transdermal rivastigmine patch for the treatment of Alzheimer's disease: a review, Int. J. Clin. Pract. 63 (2009) 799–805, https://doi.org/10.1111/j.1742-1241.2009.02052.x.
[67] Z.-Z. Yang, Y.-Q. Zhang, Z.-Z. Wang, K. Wu, J.-N. Lou, X.-R. Qi, Enhanced brain distribution and pharmacodynamics of rivastigmine by liposomes following intranasal administration, Int. J. Pharm. 452 (2013) 344–354, https://doi.org/10.1016/j.ijpharm.2013.05.009.
[68] K. Yin Win, S. Feng, Effects of particle size and surface coating on cellular uptake of polymeric nanoparticles for oral delivery of anticancer drugs, Biomaterials 26 (2005) 2713–2722, https://doi.org/10.1016/j.biomaterials.2004.07.050.
[69] B. He, P. Lin, Z. Jia, W. Du, W. Qu, L. Yuan, W. Dai, H. Zhang, X. Wang, J. Wang, X. Zhang, Q. Zhang, The transport mechanisms of polymer nanoparticles in Caco-2 epithelial cells, Biomaterials 34 (2013) 6082–6098, https://doi.org/10.1016/j.biomaterials.2013.04.053.